In-plane spectroscopy with optical fibers and liquid-filled APEX™ glass microcuvettes



2013 J. Micromech. Microeng. 23 107001

(http://iopscience.iop.org/0960-1317/23/10/107001)

J. Micromech. Microeng. **23** (2013) 107001 (6pp) doi:10.1088/0960-1317/23/10/107001

TECHNICAL NOTE

# In-plane spectroscopy with optical fibers and liquid-filled APEX™ glass microcuvettes

**William R Gaillard**[1], **Khalid Hasan Tantawi**[1,4], **Emanuel Waddell**[2], **Vladimir Fedorov**[3] **and John D Williams**[1,5]

[1] Department of Electrical and Computer Engineering, University of Alabama in Huntsville, Huntsville, AL 35899, USA
[2] Department of Chemistry, University of Alabama in Huntsville, Huntsville, AL 35899, USA
[3] Department of Physics, University of Alabama at Birmingham, Birmingham, AL 35294, USA

E-mail: john.williams@uah.edu

Received 2 April 2013, in final form 2 August 2013
Published 28 August 2013
Online at stacks.iop.org/JMM/23/107001

**Abstract**
Chemical etching and laser drilling of microstructural glass results in opaque or translucent sidewalls, limiting the optical analysis of glass microfluidic devices to top down or non-planar topologies. These non-planar observation topologies prevent each layer of a multilayered device from being independently optically addressed. However, novel photosensitive glass processing techniques in APEX™ have resulted in microfabricated glass structures with transparent sidewalls. Toward the goal of a transparent multilayered glass microfluidic device, this study demonstrates the ability to perform spectroscopy with optical fibers and microcuvettes fabricated in photosensitive APEX™ glass.

(Some figures may appear in colour only in the online journal)

## 1. Introduction

A major milestone in microfluidic technology is the realization of a reusable chemical reactor that features embedded optical fibers for optical analysis. On-chip optics improve reliability and stability through precise positioning of the source and detection optics with respect to the fluid sample. For applications such as chemical detection, particle counting, and flow characterization, it is desirable to optically examine the contents of microfluidic channels. Single layer devices can be optically addressed with a source and detector above and below the channel layer. Optical analysis in multilayered or stacked microfluidic devices requires in-line or planer observation through the sidewalls.

Many microfluidic devices today are fabricated in silicon, glass, or polymeric materials such as polydimethylsiloxane (PDMS). PDMS and other silicone rubbers are transparent, allowing for planar observation; however these polymers degrade or swell when in contact with certain chemistries [1]. While glass and silicon are more expensive and difficult to fabricate, these materials are preferred for applications where PDMS is incompatible with the required chemistry. Non-planar observation topologies are utilized for glass and silicon channels due to visibly translucent or opaque sidewalls present in these structures. Most glass channel sidewalls attain a microscale surface roughness during the chemical etching or laser drilling process necessary to pattern channels [2–5]. Conversely, post bake annealing of photosensitive glasses such as Foturan® and APEX™ reduce surface roughness providing transparent glass devices with high aspect ratios at the microscale [6–11]. These new glass processing technologies allow for chemically inert and multilayered or

[4] Present address: Department of Career Readiness-Mechatronics, Motlow College, Smyrna, TN 37167, USA.
[5] Author to whom any correspondence should be addressed.

 

stacked microfluidic devices to be developed with in-plane observation capabilities [12]. Thus, photosensitive glasses are preferred over PDMS or silicon for cases where low cost batch fabrication, optical transparency, reusability, and high chemical resistance, are required. Furthermore, glass is a good electrical insulator, allowing for high voltage electroosmotic pumping, and a moderate thermal insulator, allowing for high temperature exothermic or endothermic chemical reactions.

Optical analysis can be accomplished with an off-chip source, lens, and detection system; however, bulky external optics are difficult to align and are more expensive than fiber optic cables. On-chip optics miniaturize and simplify the total system while improving optical detection. For over a decade several methods for embedding optical fibers in PDMS devices have developed [13–15]. Laser ablation is the most common method for producing in-line fiber channels in glass [16–18]. The bottom and sides of shallow ablated channels can have single nanometer surface roughness; nevertheless, the surface roughness of the bottom and sidewalls increases with depth due to redeposition of ablated glass [5, 19–22].

Optical fibers have been incorporated along glass channels produced with wet etching techniques, but the etch depth is typically shallow and produces a wall curvature which defocuses light [23, 24]. Many microstructurable glasses such as soda-lime, fused silica, and borosilicate are utilized for standard glass microfluidic fabrication requiring a highly concentrated HF solution and a sacrificial mask (e.g. photoresist, Cr/Au, amorphous silicon, plasma enhanced chemical vapor deposition (PECVD) amorphous silicon, low-pressure chemical vapor deposition (LPCVD) polysilicon, silicon carbide, or anodically bonded single crystal silicon) [2]. Though transparent, channel depths are generally limited to less than 100 $\mu$m and are not adequate for integrating optical fibers [2, 3, 25, 26].

To achieve high optical efficiency, integration of optical fibers with glass microfluidics requires tall and transparent fluidic channels. Thus, channel height should be equal to or greater than the diameter of the fiber. A typical optical fiber with a protective coating has a diameter of 250 $\mu$m, and a bare optical fiber has a diameter of 125 $\mu$m. Shallow channels can be transparent; however, taller channels become translucent or opaque. An increase in surface roughness for deeper channels in standard glasses results from defects such as scratches, dust, or pin holes in the sacrificial mask layer, from stresses in the mask or glass, or from redeposition of insoluble products during the etch [2, 3]. Channel depths of 500 $\mu$m with optical transparency in the Vis-IR range have been demonstrated with more advanced processes. These processes include the use of high quality, optimized mask deposition to minimize mask stress and defects; pre-process annealing of the glass to remove stress; pre-etching of the glass to alleviate stress by removal of surface scratches or defects; and combinations of etchant solutions such as HF/HCl, HF/$HNO_3$, or HF/$NH_4F$ to eliminate redeposition during the etch [2, 3, 24, 27]. Nevertheless, due to the isotropic etch profile in microstructurable glass, the channel walls form half-circles or trapezoids which defocus light, thus reducing fiber-to-fiber optical coupling.

For this study, microcuvettes were utilized with in-plane optical fibers for spectroscopy. Cuvettes were patterned using photosensitive glass, which offers the advantages of reusability, chemical resistance, high aspect ratios, and optical transparency. These materials can also be easier and less expensive to work with than traditional glasses. Though fabricating deep channels in glass with optically smooth sidewalls is challenging, multiple research teams have demonstrated these processes using both Foturan [6–9] and APEX [10, 11] without the use of a sacrificial etch mask. The resulting curvature observed in these glasses actually focuses light [9, 10], and can be used to enhance fiber-to-fiber optical coupling while maintaining nearly ideal channel geometry for fluid flow. Thus, the cost and complexity is lessened, the need for external optics is reduced, and the performance is improved. Finally, this experiment demonstrates the basic requirements for developing complex lab-on-a-chip spectroscopy systems with multiple fiber aligned measurement locations.

## 2. Device description

The surface roughness of optically smooth micropatterned APEX™ glass was presented by Tantawi in a previous publication [11]. In that work laser interferometry was used to measure sidewall roughness at various locations across the thickness of the sidewalls. The sidewalls of the microcuvettes were demonstrated in [10] and [11] to have an RMS surface roughness of 33 nm and an optical transparency window between approximately 350–4500 nm. While there is no set standard, a surface roughness less than one tenth of the applied wavelength is commonly used in most optical applications. Curvature on the sidewalls results from a combination of three factors: optical diffraction, etching from both sides of the glass simultaneously, and from compressive and geometric loading [9]. Radii of curvature from approximately 2–4 mm were produced in similar 1 mm tall Foturan features [9]. The verticality of APEX™ structures is similar to that of Foruran.

In this work, microcuvettes fabricated in APEX™ photosensitive glass, and optical fibers were utilized for spectroscopy of deionized (DI) water and ethanol. Microcuvettes simulate a microfluidic channel but are easier to fill and empty. The microcuvettes were fabricated using methods outlined by Tantawi and Williams [9–11]. The walls and base were fabricated separately and thermally fused to form the microcuvette. This fusion bonding process can be repeated to create multilayered microfluidic devices. The sidewalls of the cuvettes fabricated for this study are 300 $\mu$m thick, 350 $\mu$m tall, and separated by 700 $\mu$m. Figure 1 depicts a microcuvette with optical fibers on either side. The demonstration of spectroscopy through the nearly vertical and transparent side walls of the microcuvette illustrates the superiority of photosensitive glass to other microfluidic materials.

## 3. Experiment and method

For this experiment, an APEX™ glass microcuvette rests on a three axis micron adjustment stage and a rotation

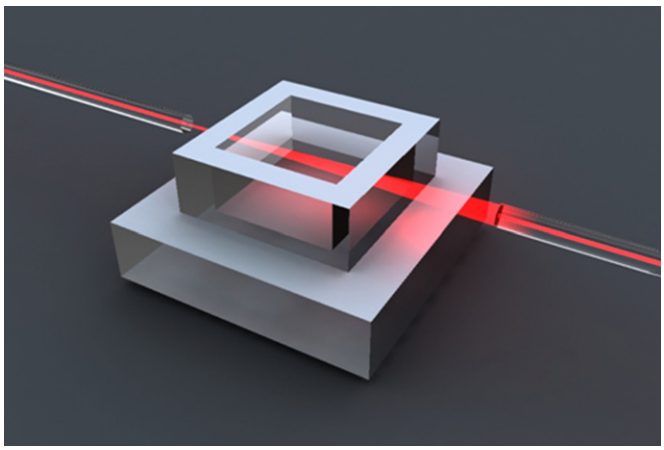

**Figure 1.** Image of a microcuvette with optical fiber source and detector on either side.

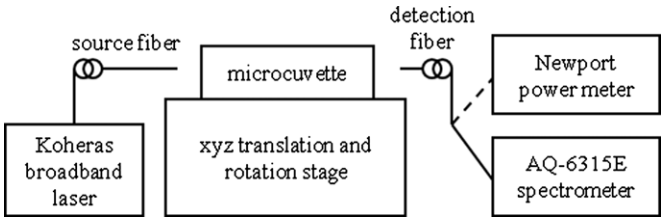


**Figure 2.** Schematic diagram of the experimental setup.

stage. Multimode optical fibers were prepared by striping the protective coating and then cleaving the ends to produce a flat fiber endface. If the fiber is not cleaved properly light will be emitted at an angle, making the alignment more difficult and reducing optical coupling. The source fiber was connected to a Koheras Super K compact white light fiber laser with emission from 500–2500 nm, and the detection fiber was connected to a Newport 2832-C dual-channel power meter with detection range from 190–1800 nm. The optical fibers were aligned using a Newport optical fiber aligner system with 15 nm precision. The fibers were first brought together until almost touching. Their positions were then adjusted until light was maximally coupled from source fiber to detection fiber. The fibers were then separated, and the cuvette was positioned in line with the fibers using the three axis and rotation stages as in figures 2 and 3.

With the cuvette in place, the detection fiber was adjusted along the optical axis of the system to find the focal point of the cuvette. The final processing step in the fabrication of the cuvettes produces slight curvature in the sidewalls which focuses light. Once the fibers were positioned to achieve maximum optical coupling, the detection fiber was removed from the optical power meter and inserted into an Ando AQ-6315E optical spectrum analyzer with detection range from 350–1750 nm. A background reference spectrum was taken with the air-filled cuvette. Next, the cuvette was filled with a liquid sample and the detection fiber was reconnected to the power meter in order to adjust the detection fiber position to compensate for the focal shift caused by the liquid. The spectrum was then obtained for the liquid and cuvette by reconnecting the detection fiber to the spectrometer.

To attain the spectra presented in this work, a Matlab program was written to determine the absorbance and percent transmission for the liquid samples. The absorbance was calculated by taking the log of the ratio of the air-filled cuvette spectrum to the liquid-filled cuvette spectrum. The percent transmission was acquired by multiplying the same ratio by 100. The built in Matlab 'smooth' function was used to filter the noise in the signals after calculating absorbance or percent transmission. This smoothing function is a moving average filter which uses a local regression method based on weighted linear least squares and a second degree polynomial model. A typical spectral plot from the Ando spectrometer contains around 1000 data points and each point on a smoothed curve was averaged based on its nearest 25 to 35 neighbors on either side.

## 4. Results and discussion

The transmission spectrum for 100% ethanol obtained with the microcuvette and fiber system is presented in figure 4, along with the spectrum obtained with a standard 1 cm quartz cuvette and Shimadzu UV-3101PC spectrophotometer. There are two notable differences between the traditional and microcuvette measurements. First, one notices a difference in transmission amplitude of the two cells. With a standard cuvette, a plane wave of light is passed through the flat cuvette walls, and the detection of the light is not dependent on incidence angle. Whereas with the microcuvette, light is emitted from a fiber, focused by the microcuvette, and the collected light

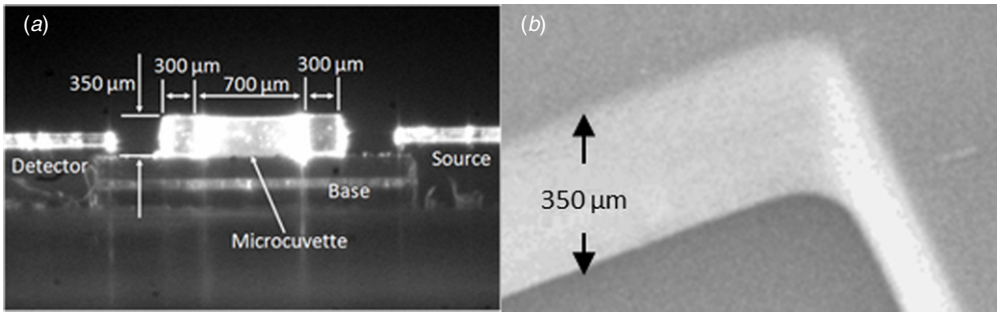


**Figure 3.** (*a*) Side view camera image with optical fiber source (right) and detector (left). The detection fiber is positioned at the focal point of the microcuvette, and shifted with respect to the axis of the source fiber due to a slightly angled source fiber endface. (*b*) SEM image of inside corner of a microcuvette.

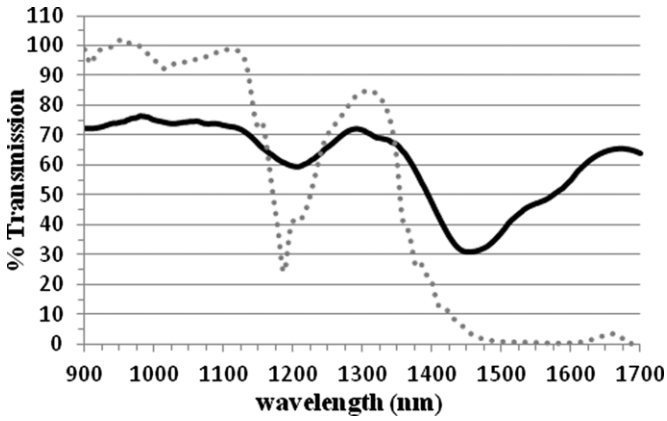


**Figure 4.** Transmission spectrum for 100% ethanol acquired with microcuvette system (solid line) and with standard quartz cuvette (dotted line).

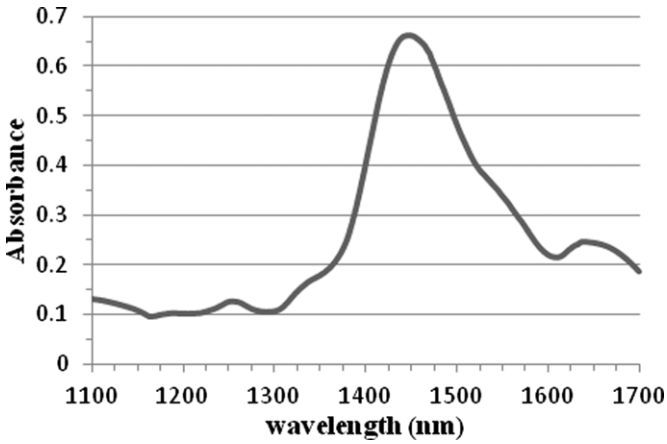


**Figure 5.** Absorbance spectrum for DI water.

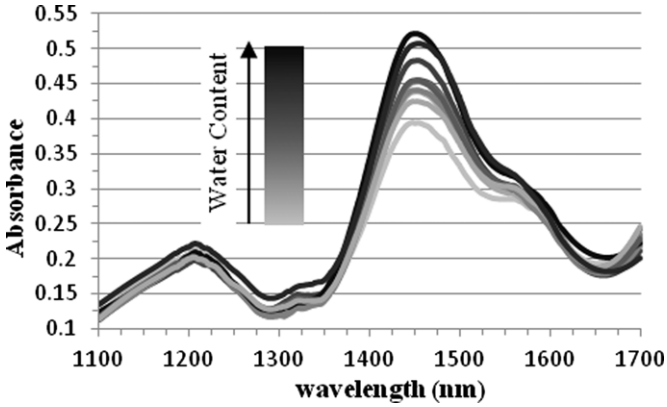


**Figure 6.** Absorbance spectrum for ethanol with varying concentrations of DI water.

is dependent on the acceptance angle of the detection fiber, and its position relative to the microcuvette focal point. Thus, less light is detected than is actually transmitted by the microcuvette and liquid sample, reducing transmission amplitude and possibly spectral resolution. Also, note the greater than 100% transmission around 950 nm for the standard cuvette is common and likely due to Fresnel reflection.

Secondly, there are similar peaks representing absorption lines of the isopropyl alcohol within the cuvettes. Both spectra show the increase in absorption at 1180 nm resulting from the second overtone of the CH stretching mode [28]. The spectra differ around 1670 nm where high transmission is found with the microcuvette and low transmission with the quartz cuvette. However, two independent studies show increased transmission in ethanol around 1670 nm when a short optical path length is used. Adachi *et al* report nearly zero absorbance with a 1 mm optical path length, and Cho *et al* report an absorbance of approximately 0.6 at 1670 nm with a 2 mm optical path length [28, 29]. The apparent strong path length dependence at 1670 nm suggests the presence of a weak absorber. The absorbing group is unknown, however; the OH group does not absorb in this region leaving the CH groups, which have overlapping absorbance bands.

Absorbance spectra were obtained for 100% DI water and for various concentrations of DI water and ethanol. In the range from 1100 to 1700 nm, the largest absorption peak results from an OH stretching mode in both DI water and ethanol at 1450 nm [28]. The peak at 1580 nm is stronger in ethanol than DI water and corresponds to a free OH overtone in ethanol. Two additional peaks are present in ethanol at 1180 and 1700 nm as a result of CH stretching modes. The absorption spectrum for DI water acquired using the mircocuvette and optical fiber system is presented in figure 5. The large peak at 1450 nm is clearly visible, while the weaker peak at 1580 nm is barely discernible for DI water.

In the time it takes to obtain a spectroscopy measurement, the liquid sample may evaporate enough to reduce the measured absorbance. The microcuvette remained full of DI water in the time needed to perform a spectroscopy experiment, but when measuring ethanol the cuvette needed to be refilled with ethanol during a measurement. Because water evaporates more slowly than ethanol, the water content of the ethanol increased in the course of a single measurement. While the absorbance curve in figure 5 can be reproduced consistently, the absorbance curves for ethanol presented in figure 6 varied slightly as a result of evaporation. The absorbance curves in figure 6 were obtained by repeating measurements in quick succession without allowing the water/ethanol to completely evaporate. Thus, the water content of the ethanol increased with each measurement. The absorption curves for ethanol remained relatively consistent between measurements except near 1450 and 1580 nm where both water and ethanol have absorption peaks. As the water content increased, the variation between the spectra increased near these two absorption maxima. The exact DI water/ethanol ratio measured is unknown, but the results demonstrate concentration sensitivity.

The spectra in figure 6 can be compared to the results from the similar studies by Cho *et al* and Adachi *et al*, where precise ratios of water and ethanol were measured and evaporation of the samples was not allowed [28, 29]. The ethanol/water spectra presented is similar to that obtained in the other studies; however, the absolute absorbance varies significantly. The variation in absolute absorbance can be explained by differences in the experiment setup where the optical path length was different in all three studies. According to the

Beer–Lambert law, the absorbance of a liquid is directly proportional to optical path length. Thus, the absolute absorbance differs by a factor corresponding to the difference in optical path length.

## 5. Conclusion and future perspectives

For microfluidic applications requiring reusability, chemical compatibility, and thermal and electrical isolation, glass is the preferred material choice over silicon or PDMS. However, many glasses are not well suited for multilayered or stacked microfluidic devices requiring in-plane observation. For optical analysis applications through the sidewalls of glass microfluidic devices, photodefinable glasses such as APEX™ are ideal. Unlike laser ablation or wet chemical etching, which produce channel walls that are either translucent or curved, APEX™ glass allows for tall, transparent, and vertical or nearly vertical sidewalls.

In this study APEX™ glass was used for the fabrication of microcuvettes utilized for the spectroscopy of DI water and ethanol. The microcuvettes simulate microfluidic channels but are easier to use for quick testing purposes. A change in the water concentration of ethanol was detected using a microcuvette and optical fiber system. This demonstration of spectroscopy with transparent microfabricated glass is a step toward microfluidic designs featuring in-plane optical analysis. Work is currently underway to design and build an all glass microfluidic device with embedded optical fibers for chemical detection. Such a device would be capable of measuring precise sample concentrations as sample evaporation would not occur.

## Acknowledgments

This research is sponsored by the Alabama EPSCoR Graduate Research Scholars Program under award number EPS-1158862, and supported by the Office of the Vice President for Research in the University of Alabama in Huntsville, Huntsville, AL 35899.

## References

[1] Lee J N, Park C and Whitesides G M 2003 Solvent compatibility of poly(dimethylsiloxane)-based microfluidic devices *Anal. Chem.* **75** 6544–54

[2] Iliescu C, Jing J, Tay F E, Miao J and Sun T 2005 Characterization of masking layers for deep wet etching of glass in an improved HF/HCl solution *Surf. Coat. Technol.* **198** 314–8

[3] Simpson P C, Woolley A T and Mathies R A 1998 Microfabrication technology for the production of capillary array electrophoresis chips *Biomed. Microdevices* **1** 7–25

[4] Malek C K, Robert L, Boy J-J and Blind P 2007 Deep microstructuring in glass for microfluidic applications *Microsyst. Technol.* **13** 447–53

[5] Ben-Yakar A, Byer R L, Harkin A, Ashmore J, Stone H A, Shen M and Mazur E 2003 Morphology of femtosecond-laser-ablated borosilicate glass surfaces *Appl. Phys. Lett.* **83** 3030–2

[6] Cheng Y, Tsai H L, Sugioka K and Midorikawa K 2006 Fabrication of 3D microoptical lenses in photosensitive glass using femtosecond laser micromachining *Appl. Phys.* A **85** 11–14

[7] Cheng Y, Sugioka K, Masuda M, Shihoyama K, Toyoda K and Midorikawa K 2003 Three-dimensional micro-optical components embedded in Foturan(R) glass by a femto second laser *Proc. SPIE* **5063** 103–7

[8] Cheng Y, Sugioka K, Masuda M, Shihoyama K, Toyoda K and Midorikawa K 2003 Optical gratings embedded in photosensitive glass by photochemical reaction using a femtosecond laser *Opt. Express* **11** 1809–16

[9] Williams J, Schmidt C and Serkland D 2010 Processing advances in transparent Foturan Glass MEMS *Appl. Phys.* A **99** 777–82

[10] Tantawi K H, Waddell E and Williams J D 2013 Structural and composition analysis of APEX™ and Foturan™ photodefinable glasses *J. Mater. Sci.* **48** 5316–23

[11] Tantawi K H, Oates J, Kamali-Sarvestani R, Bergquist N and Williams J D 2011 Processing of photosensitive APEX™ glass structures with smooth and transparent sidewalls *J. Micromech. Microeng.* **21** 017001

[12] Tantawi K H, Gaillard W, Helton J, Waddell E, Mirov S, Fedorov V and Williams J D 2013 In-plane spectroscopy of microfluidic systems made in photosensitive glass *Microsyst. Technol.* **19** 173–7

[13] Chabinyc M L, Chiu D T, McDonald J C, Stroock A D, Christian J F, Karger A M and Whitesides G M 2001 An integrated fluorescence detection system in poly(dimethylsiloxane) for microfluidic applications *Anal. Chem.* **73** 4491–8

[14] Polynkin P, Polynkin A, Peyghambarian N and Mansuripur M 2004 Evanescent field-based optical fiber sensing device for measuring the refractive index of liquids in microfluidic channels *Opt. Lett.* **30** 1273–5

[15] Tung Y-C, Zhang M, Lin C-T, Kurabayashi K and Skerlos S J 2004 PDMS-based opto-fluidic micro flow cytometer with two-color, multi-angle fluorescence detection capability using PIN photodiodes *Sensors Actuators* B **98** 356–67

[16] Schafer D, Gibson E A, Salim E A, Palmer A E, Jimenez R and Squier J 2009 Microfluidic cell counter with embedded optical fibers fabricated by femtosecond laser ablation and anodic bonding *Opt. Express* **17** 6068–73

[17] Cheng Y, Sugioka K and Midorikawa K 2005 Freestanding optical fibers fabricated in a glass chip using femtosecond laser micromachining for lab-on-a-chip applications *Opt. Express* **13** 7225–32

[18] Ke K, Ernest J, Hasselbrink F and Hunt A J 2005 Rapidly prototyped three-dimensional nanofluidic channel networks in glass substrates *Anal. Chem.* **77** 5083–8

[19] Li C and Nikumb S 2003 Optical quality micromachining of glass with focused laser-produced metal plasma etching in the atmosphere *Appl. Opt.* **42** 2383–7

[20] Sun H, He F, Zhou Z, Cheng Y, Xu Z, Sugioka K and Midorikawa K 2007 Fabrication of microfluidic optical waveguides on glass chips with femtosecond laser pulses *Opt. Lett.* **32** 1536–8

[21] Queste S, Salut R, Clatot S, Rauch J-Y and Malek C G K 2010 Manufacture of microfluidic glass chips by deep plasma etching, femtosecond laser ablation, and anodic bonding *Microsyst. Technol.* **16** 1485–93

[22] Said A A, Dugan M, Bado P, Bellouard Y, Scott A, Jose J and Mabesa R 2004 Manufacturing by laser direct-write of three-dimensional devices containing optical and microfluidic networks *Proc. SPIE* **5339** 194–204

[23] Lin C-H, Lee G-B, Fu L-M and Chen S-H 2004 Integrated optical-fiber capillary electrophoresis microchips with novel spin-on-glass surface modification *Biosensors Bioelectron.* **20** 83–90

[24] Li H-F, Cai Z W and Lin J-M 2006 Separation of catecholamines by microchip electrophoresis with a simple

integrated laser-induced fluorescence detector *Anal. Chim. Acta* **565** 183–9

[25] Lin C-H, Lee G-B, Lin Y-H and Chang G-L 2001 A fast prototyping process for fabrication of microfluidic systems on soda-lime glass *J. Micromech. Microeng.* **11** 726–32

[26] Zhu H, Holl M, Ray T, Bhushan S and Meldrum D R 2009 Characterization of deep wet etching of fused silica glass for single cell and optical sensor deposition *J. Micromech. Microeng.* **19** 065013

[27] Corman T, Enoksson P and Stemme G 1988 Deep wet etching of borosilicate glass using an anodically bonded silicon substrate as mask *J. Micromech. Microeng.* **8** 84–87

[28] Cho S, Chung H, Woo Y-A and Kim H-J 2005 Determination of water content in ethanol by miniaturized near-infrared (NIR) system *Bull. Korean Chem. Soc.* **26** 115–8

[29] Adachi D, Katsumoto Y, Sato H and Ozaki Y 2002 Near-infrared spectroscopic study of interaction between methyl group and water in water-methanol mixtures *Appl. Spectrosc.* **56** 357–61